HiSST: International Conference on
High-Speed Vehicle Science Technology
26–29 November 2018, Moscow, Russia

Structural Topology Optimisation of the HEXAFLY-INT Vertical Fin

David J. Munk[1], Gareth A. Vio[1], Dries Verstraete[1], Victor F. Villace[2], Johan Steelant[2]

Abstract

The structural design of hypersonic aircraft is a difficult task, requiring the coupling and consideration of several physical phenomena. The high flight speeds result in excessive temperatures that, along with the large aerodynamic pressures, must be sustained by the structure. Furthermore, to satisfy the stability criteria of the aircraft, the centre of gravity must not be behind the aerodynamic centre. Therefore, reducing the mass towards the backend of the vehicle is of utmost importance. Topology optimisation has matured to one of the most important aspects of structural design. Currently it is used by industry for building and bridge design. However, the highly complex, transient, multi-physics environment of hypersonic aircraft has not yet seen the application of topology optimisation. Therefore, in this study, the internal structure of the vertical fins for the High-speed Experimental Fly vehicles – International (HEXAFLY-INT) ESA led project, developing an experimental hypersonic transport aircraft, is designed using a novel discrete topology optimisation algorithm. The algorithm considers, for the first time, the transient effects of the flight trajectory to ensure a holistic design for the entire mission is developed.

Keywords: Topology optimisation, Aerothermoelastic coupling, stress, buckling

Nomenclature

Cp – Pressure coefficient
F – View factor
L, M, N – Number of variables
P – Pressure
Q – Dynamic pressure
T – Temperature
V – Volume
f, g – Constraints
h – Convective heat transfer coefficient
q – Heat transfer
t – Time
u – Dimensionless factor
$\boldsymbol{x}$ – Design variables

Greek
α – Absorptivity
ε – Emissivity
κ – Heat conduction coefficient
ρ – Density
σ – Stefan-Boltzmann coefficient
∇ – Gradient operator

Subscripts
amb – Ambient
cond – Conduction
conv – Convection
i – index
rad – Radiation
ref – Reference
stag – Stagnation
∞ – Free-stream

1. Introduction

Hypersonic flight has been explored for the past six decades, motivated by shorter flight times and reusable launch vehicles for affordable access to space [1]. The addition of significant heat transfer into the structure caused by hypersonic flight adds complexity and difficulty to the design of such vehicles. Local failure, such as panel buckling, can arise from combinations of thermal stresses and the

[1] *University of Sydney, Sydney, Australia, david.munk@sydney.edu.au, gareth.vio@sydney.edu.au, dries.verstraete@sydney.edu.au*
[2] *European Space Agency (ESA-ESTEC), Noordwijk, the Netherlands, victor.fernandez.villace@esa.int, Johan.Steelant@esa.int.*

interaction of the panels with the airflow [2]. Furthermore, nonlinear dynamic effects are magnified and can result in earlier transition to flutter and other unwanted dynamic behaviour [3, 4]. Therefore, when designing such vehicles, one cannot ignore the complex coupled environment that is present. Hence, the development of accurate computational aerothermodynamic simulation capabilities is important for the design and analysis of hypersonic vehicles.

Topology optimisation discretises the geometry of a given design domain into a number of design variables, which represent the structural properties, i.e. density and stiffness, such that the material layout or topology of the structure can be optimised for a given set of loads, boundary conditions and constraints [7]. Topology optimisation differs from conventional shape and sizing optimisation; since the design can attain any shape within the design space, rather than being limited to a pre-defined configuration where only parametric variables, such as thickness, can be changed. Topology optimisation applied to aircraft structures falls into two main categories. The first, and more common, is referred to as local design. Local design is when the design space is limited to a pre-determined layout, i.e. a given number of ribs and spars, or when only applied to local regions or subcomponents, i.e. rib leading edges. These studies aim to determine the optimal local cut-outs in a pre-defined global structure. Such studies include topology optimisation applied to single ribs [7], single panels [7], or to pre-defined rib and spar layouts [8]. The second, with fewer examples in the literature, is referred to as global design. Global design is when topology optimisation is applied to the entire wing-box structure. These studies aim to determine the layout of the major internal structural members, and usually begin with a completely solid wing, as found in [9]. Typically, unconventional or unmanufacturable structures result from global design topology optimisation, and thus, the structure may need to be converted into a more conventional aircraft design. Thus far, the literature of topology optimisation applied to aircraft structures, especially for global designs, is limited. This may be due to the complex physical environment that must be designed for, requiring accurate computational models that couple various physics.

Coupled aerothermodynamic applications to structural topology optimisation are very rare. To the best of the authors' knowledge, only Munk et al. [10] considered a coupled aerothermodynamic environment to design a hypersonic aircraft wing. Nonetheless, only one load case, cruise, was considered with a focus on the effect of different levels of coupling on the final design [10]. Therefore, the resulting design is only optimised for one load case and may perform undesirably at others. Hence, in this study, a topology optimisation algorithm that considers the transient aerothermoelastic load is developed and applied to the entire flight envelope of a hypersonic vehicle to demonstrate, for the first time, topology optimisation for a complete hypersonic application.

2. Methodology

2.1. Load case environment

To determine the temperature distribution of the vertical fin throughout the flight trajectory a transient thermal analysis is performed. The analysis must include the heat transfer due to radiation, q_{rad}, and convection, q_{conv}, from the environment to the vertical fin and the internal conduction, q_{cond}, inside the vertical fin. The heat balance is shown schematically in Fig. 1.

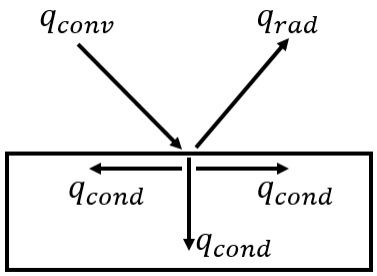

Fig 1. Heat balance for the transient thermal analysis

The heat transfer due to convection, q_{conv}, can be found from the following:

$$\mathrm{q(t)_{conv}} = h_{ref} \cdot u(t)\left[T(t) - T(t)_{stag}\right] \quad (1)$$

where h_{ref} is the convective heat transfer coefficient for the vertical fin, which is determined by a steady Computational Fluid Dynamics (CFD) simulation corresponding to Mach 7.5 along the nominal trajectory and a conservative attitude of -5° and 2° side-slip angle. The variation of the heat transfer coefficient with time, t, is implemented in the analysis through a control node, where the heat transfer rescaling factor, $u(t)$, is defined along the trajectory as:

$$u(t) = \frac{\rho \cdot v}{(\rho \cdot v)_{ref}} \quad (2)$$

This rescaling factor is derived from the assumption of calorically perfect gas and constant Stanton number along the trajectory. The reference temperature, $T(t)_{stag}$, is the stagnation temperature along the trajectory and $T(t)$ is the fin wall temperature.

To determine the heat transfer due to radiation, q_{rad}, the following equation is solved:

$$q_{rad}(t) = \sigma \cdot F \cdot [\varepsilon T(t)^4 - \alpha T_{amb}^4] \quad (3)$$

where σ is the Stefan-Boltzmann constant and is defined to be $5.67(10^{-8})$Wm^{-2}K^{-4}, F is the view factor and is assumed to be 1.0, ε is the emissivity and is taken as 0.9 since a high-emissivity paint is applied to the fin and α is the absorptivity which, for a grey body, equals the emissivity. The ambient temperature for radiative exchange, T_{amb}, is taken as a constant value of 300K.

Finally, to determine the heat transfer due to conduction, q_{cond}, Fourier's law is solved:

$$q_{cond}(t) = \kappa(T) \cdot \nabla T(t) \quad (4)$$

where κ is the materials conductivity coefficient and $\nabla T(t)$ is the temperature gradient. The conductivity of the material is a function of temperature. Eqs. (1), (3) and (4) are coupled together in a transient heat transfer analysis to determine the temperature profile of the vertical fin for the entire flight envelope. The thermal flight envelope, determined from the trajectory analysis, is depicted in Fig. 2.

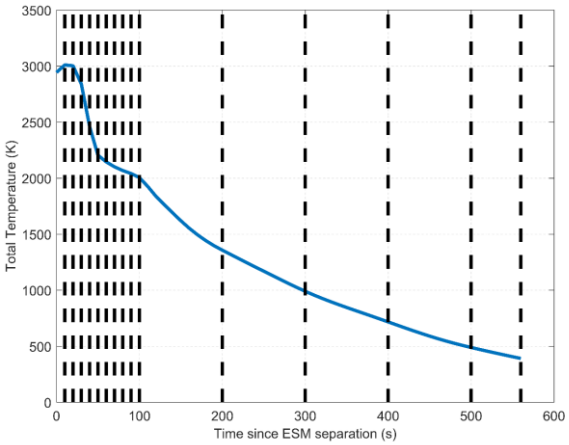

Fig 2. Thermal flight envelope for vertical fin

The loads that drive the optimal design throughout the complete trajectory are considered in a stepwise manner at the intervals indicated by the dotted lines in Fig. 2. The granularity is increased during the first 100 seconds of the flight (Fig. 2) as this period corresponds with a steeper variation of stagnation temperature, which drives the thermal load to the structure.

The thermal load cases must be complemented by the aerodynamic pressure acting on the fin. This can be determined by

$$P(t) = P_{\infty}(t) + Q(t) * Cp_{ref} \quad (5)$$

where $P(t)$ is the pressure distribution over the fin at a given time t, $P_{\infty}(t)$ is the static pressure of the flow at a given time t, $Q(t)$ is the dynamic pressure of the flow at a given time t and Cp_{ref} is the reference pressure coefficient distribution over the entire fin, determined by the CFD at Mach 7.5, -5° angle of attack and 2° side-slip angle. The static and dynamic pressures in Eq. (5) are determined along the nominal trajectory.

2.2. Topology optimisation

Topology optimisation seeks to find the best location to place structure in a pre-defined design domain that is subjected to known loading and boundary conditions, such that a pre-defined objective is maximised or minimised whilst satisfying given constraints. The problem that is dealt with here is the design of the internal structure for the vertical fins. The objective is mass minimisation, whilst satisfying the failure constraints. Therefore, the topology optimisation problem with a mass minimisation objective and various physical constraints can be stated as follows:

$$\begin{aligned} minimise: \quad & V(\boldsymbol{x}) = \sum_{i=1}^{N} x_i v_i \\ subject\ to: \ & \sigma_j(\boldsymbol{x}) \leq \bar{\sigma}_j \ \ \forall j \in [1, L] \\ & \lambda_j(\boldsymbol{x}) \geq \bar{\lambda}_j \ \forall j \in [1, L] \\ & x_i \in \{0, 1\} \ \forall i \in [1, N] \end{aligned}$$

where V is the total structural volume and v_i is the volume of the i^{th} structural element. The design variables, x_i, make up a vector, $\boldsymbol{x}$, and a stress constraint, $\bar{\sigma}_j$, and buckling constraint, $\bar{\lambda}_j$, are implemented for all L load cases. The binary design variable, x_i, represents the density of the i^{th} element. In this work, the Bi-directional Evolutionary Structural Optimisation (BESO) method [11] is employed to solve the optimisation problem.

The BESO method defines a target volume for each iteration, defined as:

$$V_{itr+1} = V_{itr}(1 \pm ER) \tag{6}$$

Where ER, known as the evolutionary ratio, is a percentage of the current structural volume, and increases or decreases V_{itr+1} towards the desired volume constraint. This, in turn, sets the threshold, α_{th}, of the sensitivity numbers. Therefore, solid elements are switched to void when:

$$\alpha_i \leq \alpha_{th} \tag{7}$$

and void elements are switched to solid when:

$$\alpha_i \geq \alpha_{th} \tag{8}$$

The amount by which the volume of the structure can increase between iterations, AR, is restricted by a maximum addition ratio AR_{max}. Once $AR > AR_{max}$, only the elements with the highest sensitivity numbers are added, such that $AR = AR_{max}$. Then the elements with the lowest sensitivity numbers are removed, in order to satisfy the target volume V_{itr+1}. The topology evolves in this way until all constraints and a convergence criterion are satisfied. The convergence criterion defined as follows:

$$\Delta O = \frac{\sum_{k=0}^{4} O_{itr-k} - \sum_{k=0}^{4} O_{itr-5-k}}{\sum_{k=0}^{4} O_{itr-k}} \leq \delta \tag{9}$$

Where δ is a pre-defined tolerance, O is the objective function, total weight in this case, and itr is the current iteration of the optimisation algorithm. Hence, the convergence criterion evaluates the change in the structural weight for the last 10 solutions. Therefore, the solution is said to be converged if the change in the objective is minimal. More details on evolutionary structural optimisation algorithms can be found in the latest textbook [12] and review paper [5] on the subject.

3. Results and Discussion

3.1. Load case environment

Using the conjugate heat transfer and CFD analysis (Sec. 2) the transient load environment for the entire flight envelope can be determined. The maximum temperatures, for different Zirconium oxide (ZrO2) thicknesses, and pressure during flight are illustrated in Fig. 3.

Three separate cases were run (Fig. 3). First, an extremely conservative approach was taken where the fin was assumed to be diving at a -4° angle of attack for the entire flight trajectory, i.e. its steepest dive. Furthermore, it was initially proposed to have a 1mm ZrO2 layer at the leading edge of the fin reducing linearly. The results for this first analysis are plotted in red in Fig. 3. The maximum temperature in the fin exceeded the titanium limit of 800°C hence it was proposed to increase the thickness of the ZrO2 layer to 2mm at the leading edge reducing linearly. The results from this second analysis are plotted in yellow in Fig. 3. This resulted in the maximum temperature coming down to under 800°C and hence was thought to be a viable option. However, the stress analysis showed that the high thermal gradients present at the leading edge resulted in stresses above the yield and ultimate of the material

at this temperature. Therefore, a less conservative approach was taken where the attitude of the vehicle throughout the flight was taken into consideration, as outlined in the Appendix. The results from this last case are illustrated by the blue line in Fig. 3. It was found that the first two analyses were too conservative, predicting a maximum temperature of over 250°C above that when the attitude of the vehicle is considered. The maximum pressure occurs 40s into the flight (Fig. 3). The pressure distribution at this time is given in Fig. 4.

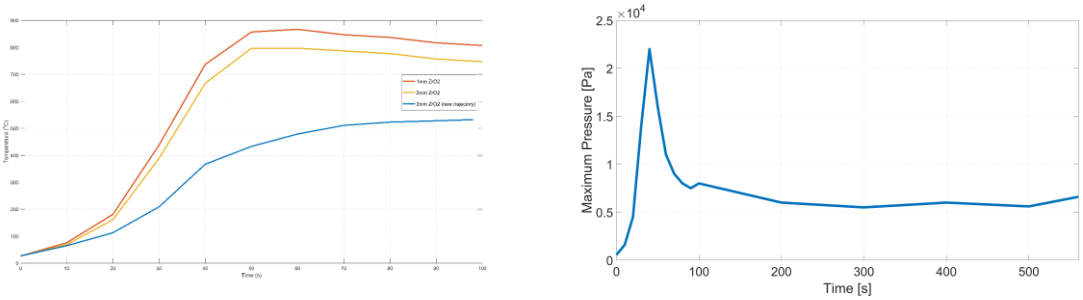

Fig 3. Maximum temperature (left) and pressure (right) of vertical fin during flight trajectory

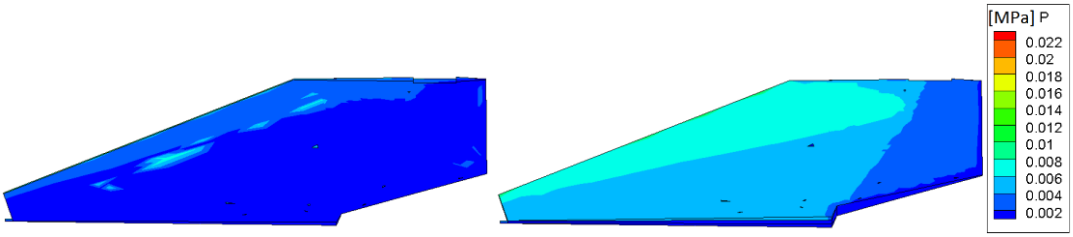

Fig 4. Pressure distribution (t=40s)

Clearly, the effect of the side slip angle can be seen (Fig. 4). On the wind side of the fin, the pressure distribution is significantly higher, compared to the protected side. Furthermore, the maximum temperature occurs 98s into the flight (Fig. 3). The temperature distribution at this time is given in Fig. 5.

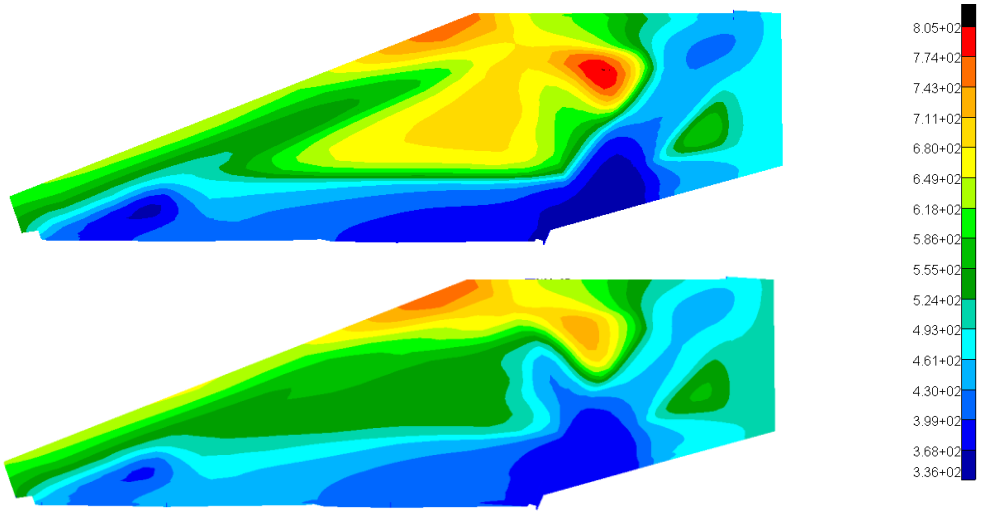

Fig 5. Temperature distribution (t=98s)

Again, the effect of the side slip angle can be seen. On the wind side of the fin the temperature distribution is significantly higher, compared to the protected side. At this time during the flight, the vehicle is pitching up therefore most of the fin is shielded by the body. The hot region toward the tip of the leading edge is due to the small amount of the fin that is unprotected from the body of the vehicle.

3.2. Topology optimisation

After applying the topology optimisation algorithm (Sec. 2.2) to the 12 manoeuvre loads the proposed design for the internal structure of the vertical fin is given in Fig. 6.

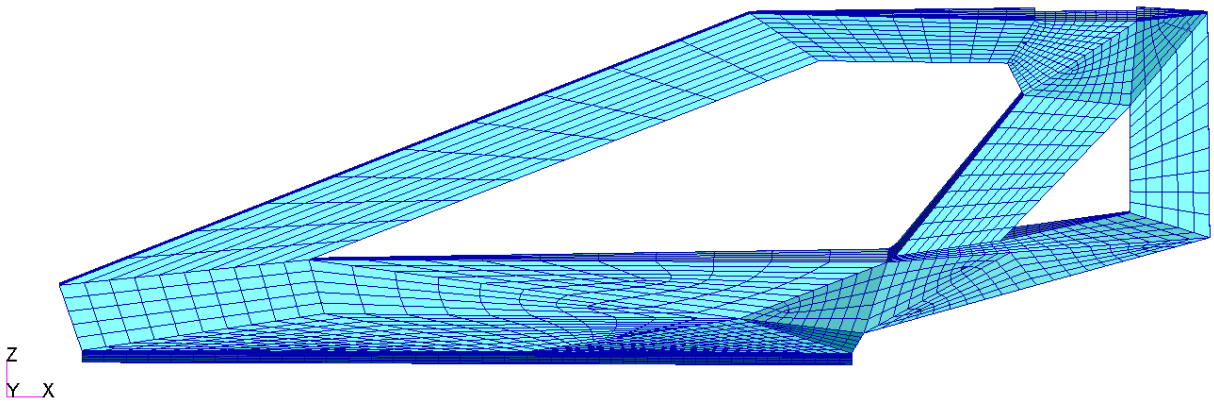

Fig 6. Proposed final internal structure for vertical fin

The final structure (Fig. 6) was determined by optimising for all 12 load cases and implementing no-designable regions towards the trailing edge where the thickness of the fin goes below a certain value such that manufacturing cut-outs in this region is not feasible and near the dovetail where cut-outs are not permitted. The final mass of the vertical fin is 12.8kg, this is a 45% weight reduction, resulting in a total weight saving of 20.88kg. In the next section it is demonstrated that this proposed structure is viable by performing a linear static and buckling analysis on the load case environment predicted (Sec. 3.1).

3.3. Validation

The pressure (Fig. 3 (right)) and temperature (Fig. 3 (left)) distributions from Sec 3.1 are applied to the vertical fin and a linear structural analysis is performed to determine the maximum stress expected in the vertical fin during flight. A summary of the maximum stress and allowable stress during the flight is given in Table 1.

Time since separation of EFTV (s)	**Maximum stress (MPa)**	**Limit stress (MPa)**	**Ultimate stress (MPa)**
10	67.8	764	862
20	75.1	764	862
30	163	666	764
40	321	588	686
47 (Beginning of pitch down)	412	539	654
50	399	546	657
60	368	515	644
70	338	483	616
80	315	464	593
90	293	456	583
98 (End of pitch down)	276	456	583

Table 1. Maximum stress in vertical fin at different time steps

The maximum stress occurs 47s into the flight (Tab. 1). The stress distribution at this time is given in Fig. 7.

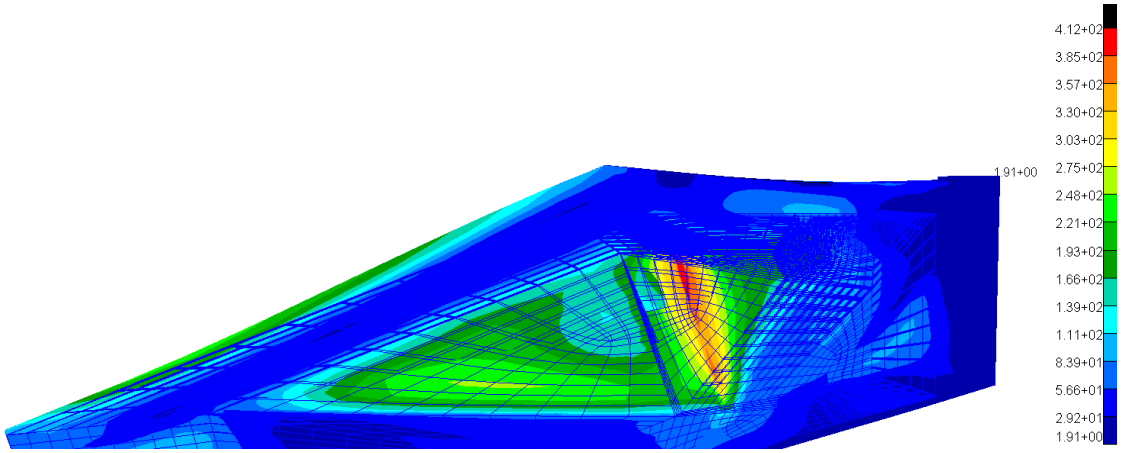

Fig 7. Stress distribution (t=47s beginning of pitch down)

The maximum stress occurs over the cavity (Fig. 7), where there is no internal structure to re-enforce the skin (Fig. 6). The worst-case yield and ultimate margins of safety are given as follows:

$$MS_{yield} = \frac{F_y}{\sigma_{max}} - 1 = 0.31$$

$$MS_{ultimate} = \frac{F_u}{1.5\sigma_{max}} - 1 = 0.06$$

The worst-case was found to be t=47s. However, both yield and ultimate margins of safety are positive indicating that the structure can withstand the loads.

Next a linear buckling solution is performed to ensure that the skin panels do not buckle under the applied pressure load cases (Fig. 3 (right)). The critical buckling mode is given in Fig. 8.

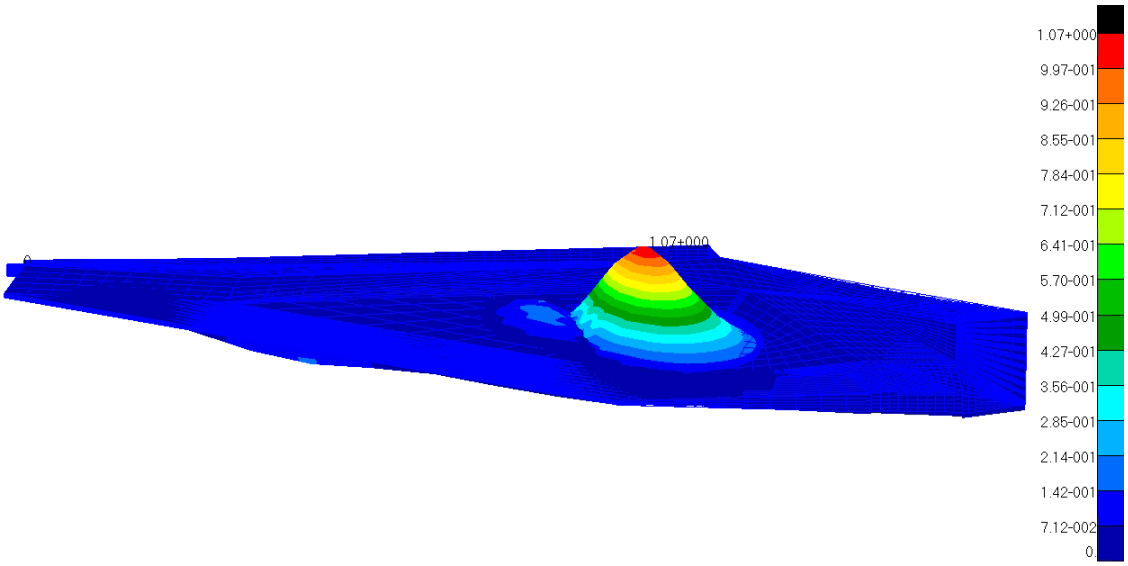

Fig 8. Critical buckling mode

The critical buckling mode for each load case is a first order bending of the main cut-out (Fig. 8). The critical buckling load factor $\lambda = \frac{F_{allowed}}{F_{applied}}$ is found to be $\lambda = 2.3951$. Therefore, buckling of the skin panels is not expected to occur.

4. Conclusion

A topology optimisation algorithm was developed and applied to the highly complex, transient, multi-physics environment of hypersonic aircraft design. A weight saving of 45% was demonstrated, reducing the mass toward the rear of the vehicle, shifting the centre of gravity forward, further stabilising the aircraft. It was demonstrated that the final design was viable, both the stress and buckling constraints were satisfied, indicating that the structure is able to sustain the expected applied loads without failure.

Furthermore, previous studies have only considered one load case in the topology optimisation algorithm, whereas, in this study, a topology optimisation algorithm that considers the transient aerothermoelastic load is developed and applied to the entire flight envelope of a hypersonic vehicle to demonstrate, for the first time, topology optimisation for a complete hypersonic application.

Appendix

A dedicated assessment of thermo-mechanical loads is necessary to ensure the survivability of the vertical tails during the intended mission. The mission of the hypersonic glider is shown in Fig. 9 with the evolution of the angle of attack (AoA), flight Mach number and sideslip angle (β) as a function of the mission elapsed time. This trajectory follows a banking manoeuvre and results from a 6DOF assessment. A dispersion analysis as a function of the mission initial conditions showed that a constant sideslip angle of β=2 or β=-2 results in a conservative assumption.

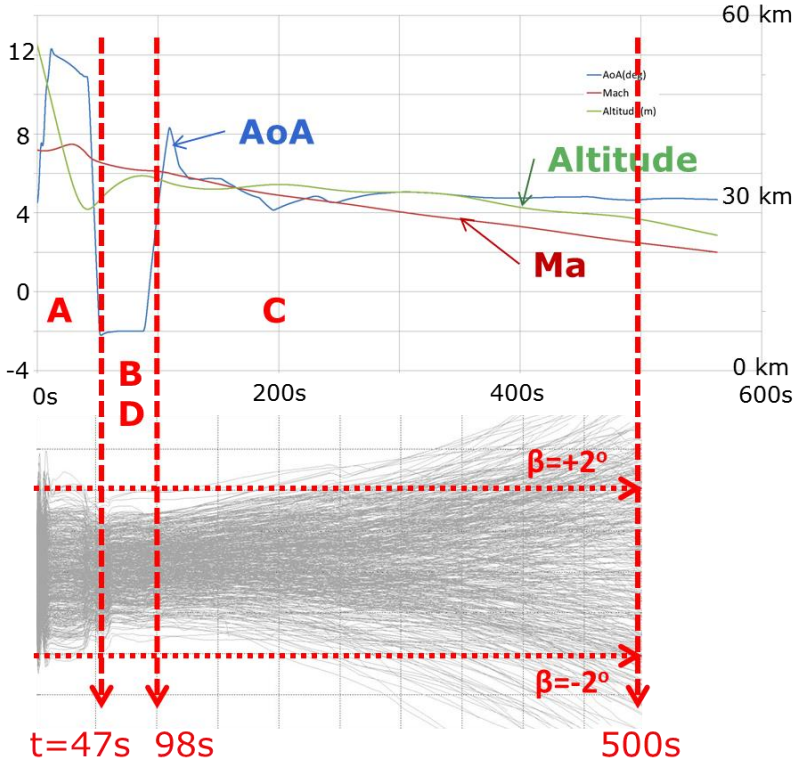

Fig 9. Mission profile (top) and sideslip angle (bottom)

Fig. 10 shows the maximum radiative-equilibrium wall temperatures on the leading edges and on each sides of the vertical tails. The data correspond to flight at Mach 7.5 and various angles of attack (AoA) and sideslip (AoS) as per the aero-thermal database.

Four conservative load cases A to D, shown in Fig. 9 and Fig. 10, were extracted based on the outlined mission profile and the aero-thermal database. Case A exhibits the maximum ΔT between starboard and port sides, whereas maximum wall temperatures are observed in case B. As such, the pressure and thermal loads from case B were considered as conservative thermo-mechanical dimensioning case for the vertical tail. Nonetheless, a first thermo-structural analysis of the vertical fin rendered thermal stresses in the region of the leading edges, which were in excess of the ultimate strength of the material (Sec. 3.1). These stresses are due to the high thermal gradients experienced by the leading edge. Therefore, the assumption of constant negative angle of attack of -5 degrees (case B) is overly conservative since it exposes the vertical tail leading edges throughout the descent trajectory.

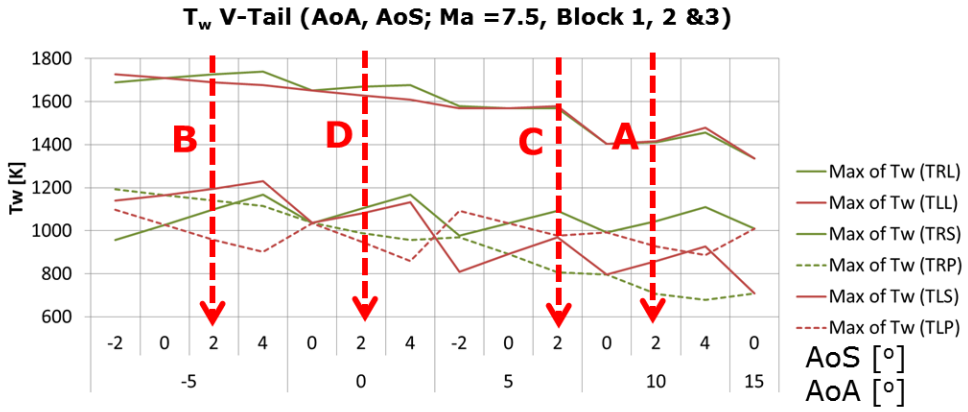

Fig 10. Maximum radiative equilibrium wall temperatures (T_w) on the leading edges (top), right tail starboard and portside (TRS & TRP) and left tail starboard and portside (TLS & TLP)

A second load case was therefore issued to assess the survivability of the vertical tail under less stringent conditions. Being the stresses driven by the thermal gradients across the leading edge, the critical load cases, which render maximum gradients between leading edge and the lateral panels are (see Fig. 10 and Table 2):

- Case A (0<t<47): on the portside of the starboard side vertical tail
- Case B (47<t<98): on the portside of the portside vertical tail
- Case C (98<t): on the portside of the starboard side vertical tail

	AEDB	Ma	AoA	AoS	ρ	v	Cp	$T_{t\infty}$
	#ID		°	°	[g/m^3]	[m/s]	[J/kg/K]	[K]
A	151-02	7.5	10	2	7.3	2325	1012	2914
B	147-02	7.5	-5	2	7.3	2325	1011	2914
C	176-01	7.5	5	2	7.3	2325	1011	2914

	AEDB	(ρ v)	$(\sqrt{\rho}\, v^3)$	$(\sqrt{\rho}\, v^3)/T_{t\infty}$
	#ID	[kg/s/m^2]	[kg$^{0.5}$ s^{-3} m$^{3/2}$]	[kg$^{0.5}$ s^{-3} m$^{3/2}$ K^{-}]
A	151-02	17.017	1075683159	369143
B	147-02	17.017	1075683159	369143
C	176-01	17.017	1075683159	369143

Table 2. Flight conditions corresponding to the critical load cases

It can be noticed that the load case is not symmetrical: critical loads are expected on each starboard or portside vertical tail at different points along the trajectory. This would require two different thermos-structural computations for each load set on the starboard or the portside vertical tail. Nonetheless, a combined load case was defined over the same vertical tail in order to perform a single thermos-structural analysis and hence spare resources. To this end, the convective heat transfer maps on each starboard and portside vertical tails corresponding to the temporal sequence of cases A to C were spatially overlapped onto the same vertical tail.

A further consideration concerns the scaling of the convective heat transfer (h_c) obtained at Ma 7.5 along the trajectory. Under the assumption of constant Stanton number (St), the viscous heat load scales with the mass flux (ρ v):

$$h_c = \frac{\dot{q}}{(T_{t\infty} - T_w)} = St\,(\rho\, v\, C_p)_\infty$$

$$\frac{h_c}{h_{c\,ref}} = \frac{\rho\, v}{(\rho\, v)_{ref}}$$

Where ($_{ref}$) refers to the Ma 7.5 reference conditions at which the convective heat transfer was obtained, the freestream density, velocity and specific heat at constant pressure are respectively ρ, v and C_p, $T_{t\infty}$ is the freestream stagnation temperature and T_w the radiative equilibrium wall temperature. It should be noted that the specific heat was assumed constant in the above derivation of the convective-heat scaling-factor.

On the other hand, the heat load experienced by the leading edge in the surroundings of the stagnation region, scales as $\rho^{0.5}\, v^3/T_{t\infty}$ (hot wall correction considered):

$$h_c \propto \rho^{0.5} v^3 / T_{t\infty} \quad (q \propto \rho^{0.5} v^3 (h_{t\infty} - h_w)/ h_{t\infty})$$

A conservative scaling (f) was thus defined taking the maximum of the viscous and stagnation scaling along the trajectory

$$f=\frac{h_c}{h_{c\,ref}} = \max\left(\frac{\rho\, v}{(\rho\, v)_{ref}}, \frac{\rho^{0.5}\, v^3}{(\rho^{0.5}\, v^3)_{ref}} \frac{(T_{t\infty})_{ref}}{T_{t\infty}}\right)$$

This confirms the viscous scaling as a conservative assumption along the trajectory profile (Fig. 11). Only during the initial part of the descent and up the reference condition (f=1) the stagnation scaling ($\rho^{0.5} v^3/T_{t\infty}$) yields a more conservative load.

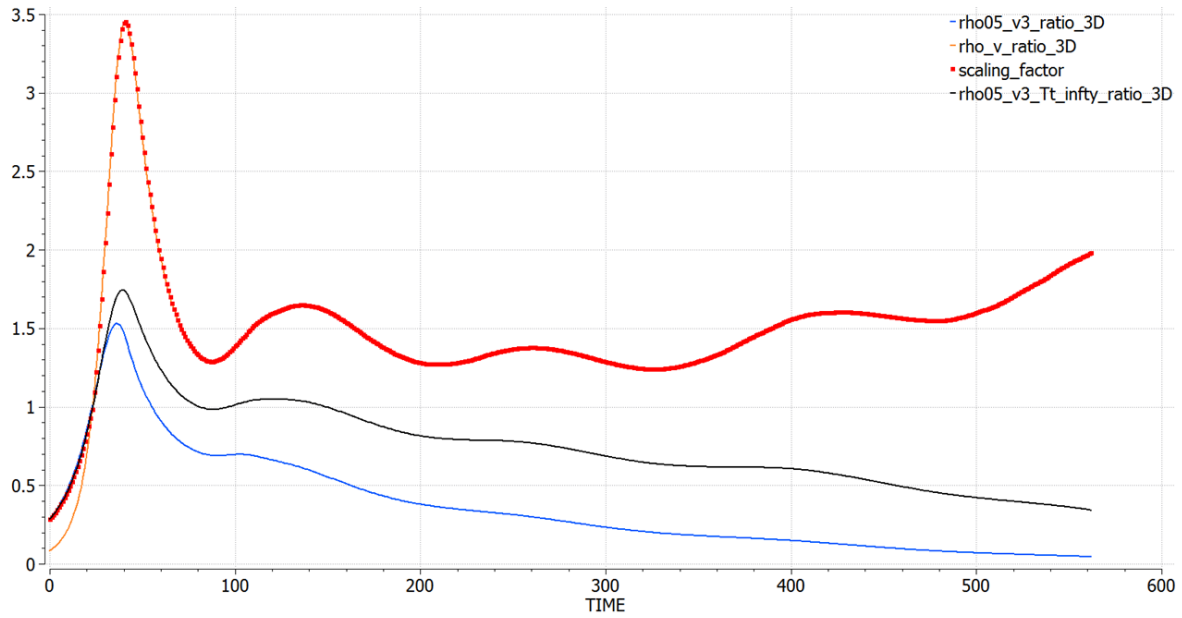

Fig 11. Scaling of the thermal loads along the trajectory

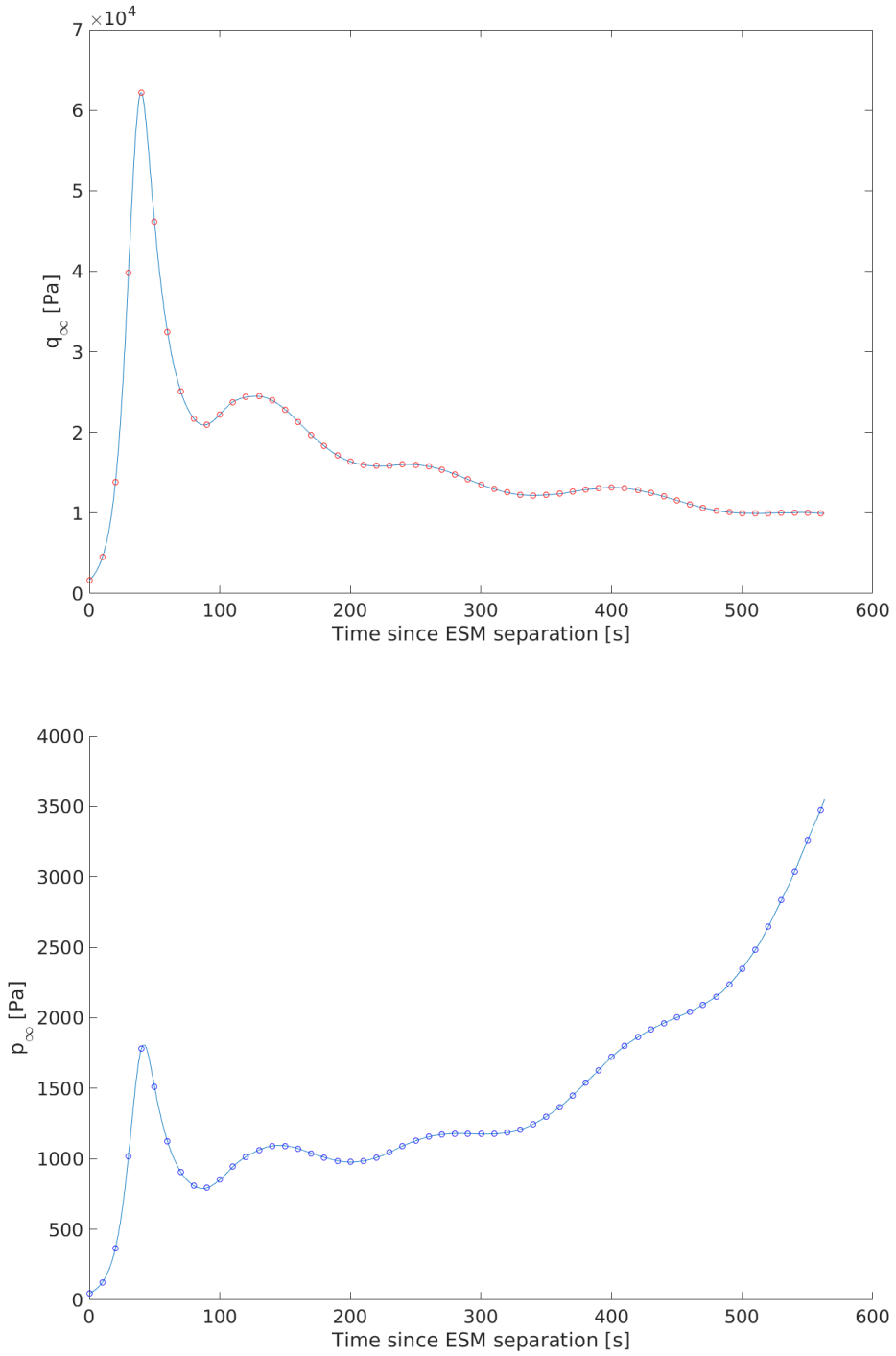

Fig 12. Dynamic and static pressures along during the banking manoeuvre

References

1. Dolvin, D.J.: Hypersonic international flight research and experimentation (HIFiRE), fundamental sciences and technology development strategy. In: 15th AIAA International Space Planes and Hypersonic Systems and Technologies Conference, AIAA Paper 2008-2581 (2008)
2. Livne, E.: Aeroelasticity of nonconventional airplane configurations – past and future, J. Aircr., 40, 1047-1065 (2003)

3. Munk, D.J., Vio, G.A., Verstraete, D.: Response of a three-degree-of-freedom wing with stiffness and aerodynamic nonlinearities at hypersonic speeds, Nonlinear Dynam., 81, 1665-1688 (2015)
4. Vio, G.A., Munk, D.J., Verstraete, D.: Transient temperature effects on the aerothermoelastic response of a simple wing, *Aerospace*, 5 (3), 71-87 (2018)
5. Munk, D.J., Vio, G.A., Steven, G.P.: Topology and shape optimization methods using evolutionary algorithms: a review, Struct. Multidiscip. Optim., 52, 613-631 (2015)
6. Maute, K., Reich, G.W.: Integrated multidisciplinary topology optimisation approach to adaptive wing design, J. Aircr., 43, 253-263 (2006)
7. Stanford, B., Beran, P., Bhatia, M.: Aeroelastic topology optimization of blade-stiffened panels, J. Aircr., 51, 938-944 (2014)
8. Stanford, B., Dunning, P.D., Optimal topology of aircraft rib and spar structures under aeroelastic loads, J. Aircr., 52, 1298-1311 (2015)
9. Dunning, P., Stanford, B., Kim, H.: Coupled aerostructural topology optimization using a level set method for 3D aircraft wings, Struct. Multidiscip. Optim., 51, 1113-1132 (2015)
10. Munk, D.J., Verstraete D., Vio, G.A.: Effect of fluid-thermal-structural interactions on the topology optimization of a hypersonic transport aircraft wing, J. Fluid Struct., 75, 45-76 (2017)
11. Huang, X., Xie, Y.: Convergent and mesh-independent solutions for the bi-directional evolutionary structural optimization method, Finite Elem. Anal. Des., 43, 1039-1049 (2007)
12. Huang, X., Xie, Y.: Evolutionary topology optimization of continuum structures: methods and applications, John Wiley & Sons, West Sussex (2010)

